Human Vision and Electronic Imaging. Proceedings of SPIE (1996), 2674, 119-130.

Visual Detection Following Retinal Damage: Predictions of an Inhomogeneous Retino-Cortical Model

Thomas L. Arnow† and Wilson S. Geisler‡

Conceptual MindWorks Inc.†, San Antonio, TX 78228
Center for Vision and Image Sciences‡ and Depart. of Psychology‡, University of Texas, Austin, TX 78712

ABSTRACT

A model of human visual detection performance has been developed, based on available anatomical and physiological data for the primate visual system**.** The inhomogeneous retino-cortical (IRC) model computes detection thresholds by comparing simulated neural responses to target patterns with responses to a uniform background of the same luminance. The model incorporates human ganglion cell sampling distributions; macaque monkey ganglion cell receptive field properties; macaque cortical cell contrast nonlinearities; and a optimal decision rule based on ideal observer theory. Spatial receptive field properties of cortical neurons were not included. Two parameters were allowed to vary while minimizing the squared error between predicted and observed thresholds. One parameter was decision efficiency, the other was the relative strength of the ganglion-cell center and surround. The latter was only allowed to vary within a small range consistent with known physiology. Contrast sensitivity was measured for sinewave gratings as a function of spatial frequency, target size and eccentricity. Contrast sensitivity was also measured for an airplane target as a function of target size, with and without artificial scotomas. The results of these experiments, as well as contrast sensitivity data from the literature were compared to predictions of the IRC model. Predictions were reasonably good for grating and airplane targets.

Keywords: spatial vision, contrast sensitivity, ganglion cells, detection, peripheral vision, retinal scotoma.

1.0 INTRODUCTION

We have developed a model of human spatial pattern detection which is based upon known optical, anatomical and electrophysiological properties of the primate visual system. The current version of the model generates predictions for the detectability of arbitrary spatial luminance patterns, presented at arbitrary retinal locations against a uniform background. The unique features of the model are: (1) a close adherence to objective optical, anatomical and electrophysiological data, (2) a truly inhomogeneous structure; e.g., the modeled properties of the retinal ganglion cells change continuously with eccentricity, and (3) the inclusion of realistic neural noise and an optimal decision mechanism.

To test the model, we compared its predictions with measurements of contrast sensitivity for sinewave grating patterns as a function of spatial frequency, target size, and retinal eccentricity. Predictions are shown for the contrast sensitivity data of Robson and Graham[1] and Arnow and Geisler[2]. We also show predictions (but no data) for the detection of sinewave grating targets assuming sharply defined retinal scotomas of various sizes and eccentricities. Finally, we show measurements of (and predictions for) the detectability of an "airplane" target as a function of its size, and the size of an artificial scotoma which obscured part of the airplane. We begin by describing the specific components of the model, and how predictions were generated.

2.0 INHOMOGENEOUS RETINO-CORTICAL MODEL

2.1 Optics of the eye.

The optical quality of the retinal images formed in the well-accommodated eye are adequately described by a single point-spread function (PSF), at least for the central 12°-15° of visual field.[3,4] In generating predictions we used the point-spread function reported by Campbell and Gubisch[5], for a 3 mm pupil. (Specifically, we represented the shape of the PSF as the sum of two Gaussians fit to the Campbell and Gubisch data; see ref. [6].) The Campbell and Gubish PSFs were measured with white light, and hence represent the effects of monochromatic and chromatic aberrations. We modeled the retinal image by convolving the Campbell and Gubisch PSF with the input stimulus.

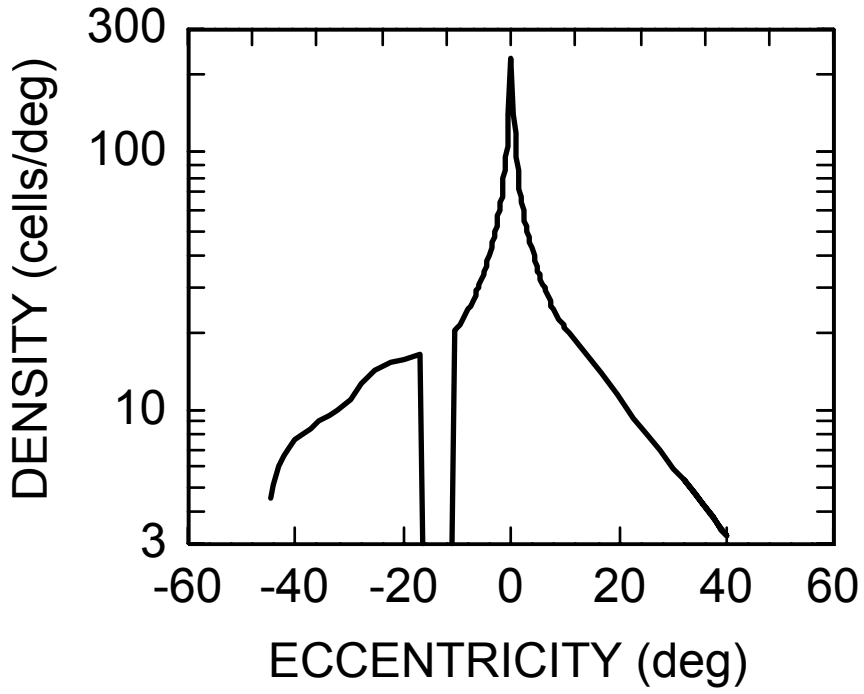

Figure 1. Density of ganglion cells along the horizontal meridian of the human eye (adapted from Curcio and Allen[7]). Positive eccentricities are the temporal retina. Under the assumptions that parvo ganglion cells constitute 80% of all ganglion cells, and that half the ganglion cells have on-centers, the peak density of on-center parvo cells is 145 cells/deg.

2.2 Ganglion cell sampling array

The output neurons of the retina are the retinal ganglion cells. Therefore, we can adequately model the effect of retinal processing on pattern detection if we can adequately model the responses of the ganglion cells. To model the responses of the ganglion cells we need to know how they sample the retinal image. It is well known that the ganglion cells sample the retinal image densely in the fovea and sparsely in the periphery. Figure 1 shows the density of the ganglion cells as a function of retinal eccentricity, based upon the recent anatomical measurements by Curcio and Allen[7] for the adult human retina[4]. Figure 1 is representative of the human retina, although there are individual differences. As can be seen, the density decreases smoothly from a value of approximately 230 cells per deg in the central fovea to under 5 cells per degree in the far periphery.

We modeled the ganglion cell sampling array directly from the function shown in Figure 1, for the temporal retina. In the version of the model reported here, we only included the parvo (midget) ganglion cells, since they appear to play the dominant role in standard contrast sensitivity experiments.[8] We assumed that the parvo cells constitute 80% of all the ganglion cells, that half of the parvo cells are on-center and half are off-center, and that on-center and off-center cells sample the same spatial locations.

The first cell in the model lattice was placed at the center of the fovea. The rest of the cells were located on concentric rings. The eccentricity of the first ring was set equal to the ganglion cell spacing (1/density) of the on-center parvo cells in the center of the fovea. The eccentricities of the other rings were derived iteratively by setting the eccentricity of the i^{th} ring equal to the eccentricity of the $i\text{-}1^{th}$ ring, plus the value of ganglion cell spacing at the $i\text{-}1^{th}$ eccentricity. Cells were equally spaced around each ring with the density appropriate for the eccentricity of the ring.

2.3 Ganglion cell receptive field properties

To generate predictions we also need to specify how each cell in the ganglion-cell lattice responds to spatial patterns in the retinal image. There have been very few electrophysiological measurements of ganglion cell responses in the human retina, and therefore we based our model upon electrophysiological and anatomical measurements in the retina and LGN of macaque monkey and upon anatomical measurements in the human retina. (The rationale for using macaque data is that the macaque visual system appears to be anatomically and psychophysically similar to that of the human. Also, for present purposes, we treat ganglion cells and LGN cells as equivalent, since their response properties are so similar.)

A number of electrophysiological studies[9,10,11] have shown that spatial receptive fields of on-center parvo ganglion cells (and parvo LGN cells) are well described by a difference-of-Gaussians function:

$$h(x,y) = \frac{\alpha}{2\pi\sigma_c^{\,2}}\exp\left(-\frac{x^2+y^2}{2\sigma_c^{\,2}}\right) - \frac{(1-\alpha)}{2\pi\sigma_s^{\,2}}\exp\left(-\frac{x^2+y^2}{2\sigma_s^{\,2}}\right) \qquad (1)$$

where $_c$ is the space constant (standard deviation) for the center, $_s$ is the space constant for the surround, and is the relative strength of the center and surround. (The equation obtained by multiplying the right side of equation (1) by -1 would describe the receptive field of an off-center ganglion cell.) Further, these studies found that parvo ganglion cells respond linearly with contrast, up to moderate contrasts. Saturation and thresholding nonlinearities appear at high contrasts, but have little effect for the contrasts near behavioral detection threshold.

Anatomical and electrophysiological studies[11,12,13] suggest that the diameters of the center mechanisms of parvo neurons are approximately equal to the spacing between the ganglion cells. Therefore, we assumed that $_c$ at each eccentricity was equal to one half the on-center (or equivalently off-center) ganglion cell spacing at that eccentricity. In the center of the fovea this translates to $_c$ = 0.21 arc min.

Electrophysiological studies[9,11] indicate that the center diameter is approximately 6 times the surround diameter, at all eccentricities. Thus, we assumed that $_s$, at each eccentricity, was 6 $_c$.

Finally, electrophysiological studies[9,11] report that the relative strength of the center and surround, , averages about 0.6. We did not keep rigidly fixed, but allowed it to vary within the physiologically plausible range of 0.5 to 0.7. The reason is that the estimated relative strength of center and surround is dependent upon the temporal properties of the stimulus (brief or high frequency stimuli tend to yield larger values of). This was one of only two free parameters in the model.

For our linear receptive-field model, the predicted response of each ganglion cell can be obtained by multiplying the retinal image by the cell's receptive field profile and integrating. Unfortunately, because the receptive fields are different at each eccentricity, fast Fourier transform techniques cannot be used to speed up the calculations.

However, for the special case in which the stimuli consist of smoothly dampened sinusoidal gratings, there is a simple approximation that greatly speeds the calculations. A smoothly dampened sinewave grating is described by a function of the form

$$L(x,y) = A(x,y)\sin\left(2\pi(ux+vy)+\phi\right)+\bar{L} \tag{2}$$

where *A(x,y)* is the dampening function, *u* and *v* are the horizontal and vertical spatial frequencies, is the phase, and $\bar{L}$ is the mean luminance. For the purpose of computing the response of a ganglion cell with a receptive field centered at x_i, y_i, the stimulus is adequately approximated by

$$L(x,y) = A(x_i,y_i)\sin\left(2\pi(ux+vy)+\phi\right)+\bar{L} \tag{3}$$

as long as *A(x,y)* is sufficiently smooth in the neighborhood of x_i, y_i. The response, g_i, of the on-center ganglion cell at x_i, y_i to this approximate stimulus is given directly by the equation

$$g_i = H(u,v)A(x_i,y_i)\sin\left(2\pi(ux_i+vy_i)+\phi\right)+H(0,0)\bar{L} \tag{4}$$

where *H(u,v)* is the Fourier transform of the receptive field profile,

$$H(u,v) = \alpha\exp\left(-2\pi^2{\sigma_c}^2\left(u^2+v^2\right)\right)-(1-\alpha)\exp\left(-2\pi^2{\sigma_s}^2\left(u^2+v^2\right)\right) \tag{5}$$

The predictions reported here for sinewave grating experiments were first obtained using the approximation (Equations 4 and 5). We then verified that the predictions were accurate by computing predictions for selected stimuli using the exact method (multiplication and integration). Predictions for the complex pattern (the airplane) were obtained using the exact method. Similar equations were used to obtain off-center ganglion cell responses.

2.4 Light adaptation

There is substantial physiological and psychophysical evidence for the existence of multiplicative and subtractive light adaptation mechanisms in the human and monkey retina.[4] The evidence suggests that light adaptation effectively subtracts from the input image approximately 90% of the mean luminance, and scales the result by a factor which gradually becomes proportional to mean luminance as mean luminance increases. These adaptation mechanisms are easily incorporated into the IRC model. However, we do not discuss them further because they only play a role when mean luminance is varied, and hence do not affect the predictions reported here.

2.5 Cortical nonlinearities and selective tuning characteristics

Several physiological properties of primary visual cortex (V1) were also included in the model because they seem certain to have important effects on detection performance. The first property is that cortical neurons have near zero response in the dark and to uniform backgrounds. Therefore, we assumed that there is an neural threshold (or subtractive adaptation) just large enough to eliminate the response to the uniform background and any spontaneous activity. The second property is that cortical cells respond in an accelerating nonlinear fashion at low contrasts. On average, the contrast response functions of cortical cells are described at low contrasts by a power function with an exponent n of approximately 2.5.[14,15] Therefore, we applied an exponent of 2.5 to the thresholded responses of the ganglion cell outputs. The combined effect of the neural threshold and the exponent is given by

$$r_i(T) = \max\left(g_i(T) - g_i(B), 0\right)^n \tag{6}$$

$$r_i(B) = \max\left(g_i(B) - g_i(B), 0\right)^n = 0.0 \tag{7}$$

where T refers to the target stimulus and B the comparison stimulus (i.e., th background alone).

Two other important characteristics of primary visual cortex were not included in this version of the model: the contrast normalization characteristics of cortical neurons,[16,17] and the selective tuning characteristics of cortical neurons for spatial frequency and orientation.[18] Contrast normalization was excluded because its most important influences should be for pattern detection against high contrast patterns (although it should still have some effect on detection against uniform backgrounds). The selective tuning characteristics of cortical cells were excluded under the assumption that the sampling of spatial frequency and orientation by cortical cells is sufficient to encode the detection information provided by the LGN cells. In other words, we made the assumption that detection performance (against uniform backgrounds) is not limited by the tuning characteristics of cortical neurons, but by the information provided by the retina via the LGN. This is not entirely unreasonable given the huge number of V1 neurons per ganglion cell.

2.6 Neural noise

The last physiologically motivated component of the model is a neural noise mechanism. Neurons in primary visual cortex, and in other cortical areas, have the property that the variance in the number of spikes produced by a stimulus is approximately proportional the mean response produced by that stimulus.[19,20] Therefore, we assumed that the variance in the response of each neuron was proportional to its mean response with a proportionality constant, K, of 1.5 (the average found in the primary visual cortex).

2.7 Optimal decision mechanism

Little is known about how central brain mechanisms pool neural information in detecting a target. However, the most parsimonious hypothesis is that the information from every relevant neuron contributes to the decision process.

Consider first a single neuron. If detection were based upon only the i^{th} neuron, and if the responses of the neuron were being used optimally, then the proportion of correct responses, P_c, would be given by the following formulas:

$$P_c = \Phi\left(\frac{d'_i}{2}\right) \tag{8}$$

$$d'_i = \frac{\left|r_i(T) - r_i(B)\right|}{\sqrt{\frac{K}{2}\left(r_i(T) + r_i(B)\right)}} \tag{9}$$

where $\Phi(\,)$ is the normal integral function. Notice that the numerator of d'_i is the absolute value of the difference in the mean responses and the denominator is the square root of the average variance of the responses. Thus, d'_i is the number of standard deviations between the mean responses to the target-plus-background and the background alone. In the typical detection task, threshold is defined as the contrast of the target which produces some criterion response accuracy (usually 70% or 75% correct). In a single-interval 2AFC task, 70% correct corresponds to a d'_i of 1.0. Thus, the predicted detection threshold, based upon the response of a single neuron, can be obtained by setting d'_i to 1.0 in equation (9) and solving for the contrast of the target.

Now consider the entire population of neurons. If the responses of the neurons are statistically independent (which we assume), and if all of the responses are combined optimally, then the value of d' for the entire population is given by

$$d' = \sqrt{\sum d'^{\,2}_i} \tag{10}$$

(see ref [21]). Predicted detection thresholds, based upon the entire population, are obtained by setting d' to 1.0 in equation (10) and solving for the contrast of the target. We have found that this optimal decision rule predicts thresholds that are substantially smaller than those observed, so we introduce a second free parameter, an efficiency parameter, , whose primary effect is to scale the predicted threshold functions, without changing predicted shape. The value of d' when the efficiency parameter is included is

$$d' = \sqrt{\varepsilon \sum d'^{\,2}_i} \tag{11}$$

If the efficiency is 1.0 equation (11) reduces to equation (10).

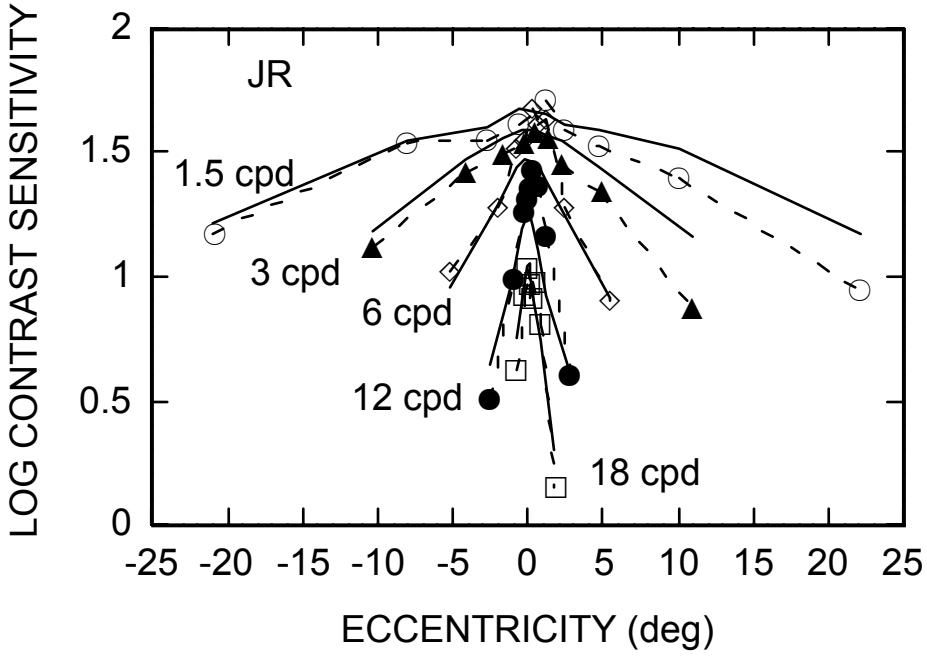

Figure 2. Contrast sensitivity for sinewave grating targets as a function of spatial frequency and retinal eccentricity (data from Robson and Graham[1]). The targets were a fixed number of cycles in size and were presented for approximately 150 ms. The solid curves are the predictions of the IRC model.

3.0 RESULTS

3.1 Predictions for sinewave grating targets

Predictions of the IRC model were generated for sinewave grating targets as a function of spatial frequency, retinal eccentricity, grating target size, and the size and location of sharply defined retinal scotomas.

Figure 2 shows contrast sensitivity data reported by Robson and Graham[1]. Each set of data points shows contrast sensitivity as function of retinal eccentricity, for the target spatial frequency indicated at the side. The grating targets were a fix number of cycles in size (approximately 4 periods x 4 periods), and were smoothly dampened at the edges (the exact stimulus specifications were used in generating predictions). Retinal eccentricity varied along the vertical meridian. The targets were presented for a duration of approximately 150 ms. The solid curves show the predictions of the IRC model with a center-to-surround weighting ( ) of 0.56. As can be seen, the model accounts for the major features of the data. The most noticeable mismatch occurs in the superior visual field. The mismatch might be explained by the fact that in the current version of the model the ganglion cell lattice is radially symmetric when, in fact, the density of ganglion cells is greater in the inferior visual field (superior retina) than in the superior visual field (inferior retina). This density difference will produce greater contrast sensitivity in the inferior visual field (as observed). A quantitative test would require constructing ganglion cell lattices that incorporate the asymmetries.

Robson and Graham's[1] measurements of contrast sensitivity as a function of sinewave target size are shown in Figure 3. They made measurements for three target spatial frequencies, at two eccentricities, for

gratings 4 cycles in height and ranging from 2 to 64 cycles in length. The solid curves show the predictions of the IRC model, with the same parameters. Again the model accounts for the major features of the data: the increase in sensitivity with number of cycles, the difference in sensitivity across spatial frequency, and the differences in sensitivity at the two eccentricities.

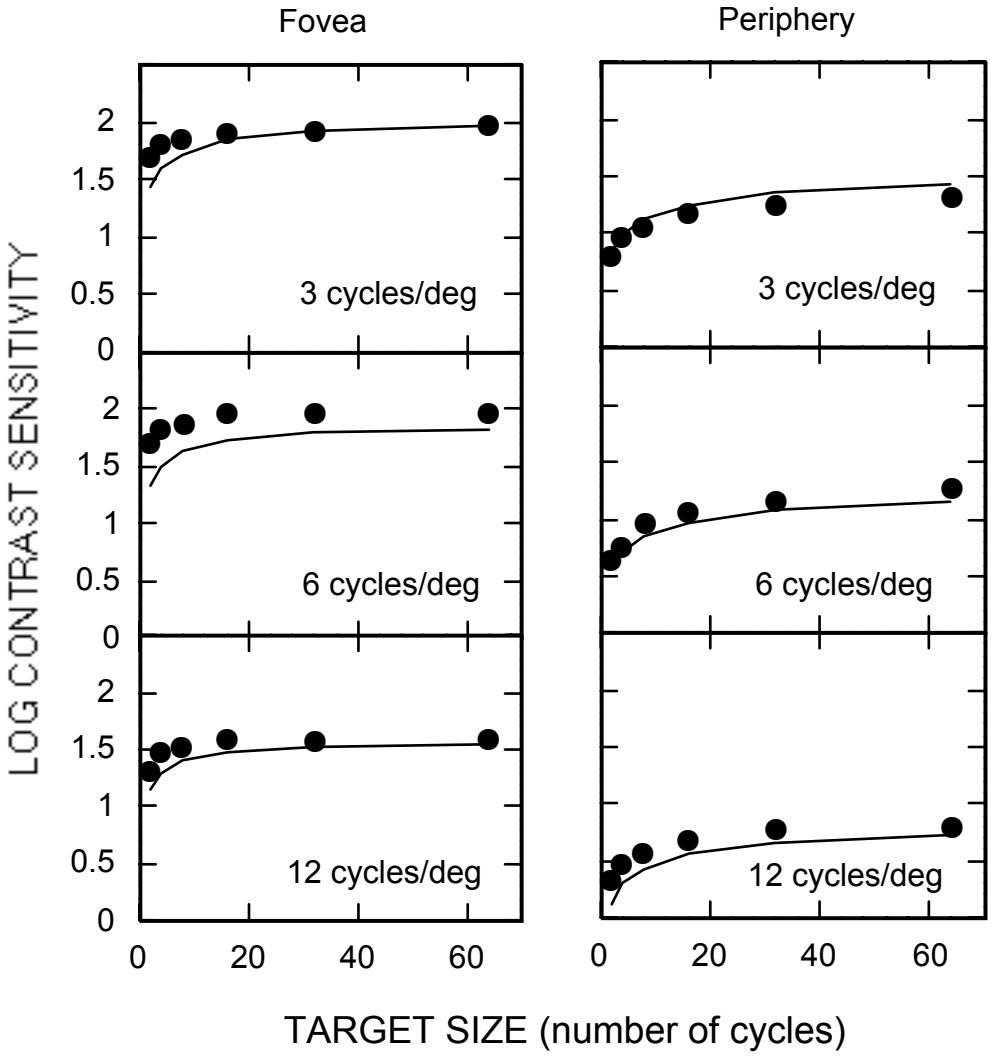

Figure 3. Contrast sensitivity for sinewave grating targets as a function of target size, spatial frequency and retinal eccentricity (data from Robson and Graham[1]). The targets were presented for approximately 150 ms. Peripheral targets were centered at 42 periods from fixation. The solid curves are the predictions of the IRC model.

Figure 4 shows contrast sensitivity measurements for sinewave grating targets as a function of spatial frequency and eccentricity for two subjects.[2] The gratings were Gaussian-dampened in all directions (bandwidth 0.5 octaves), and were in sine phase with respect to the Gaussian envelope. The targets were displayed for 200 msec on a calibrated 10-bit gray-scale monitor (white phosphor), at a mean luminance of 130 cd/m^2. Responses were collected using a 2AFC, 3-down/1-up staircase procedure; thresholds were computed from the recorded responses using a maximum-likelihood method. Subjects viewed the display with the right eye and natural pupils. Eccentricity was varied by moving the display with respect to the fixation point, and spatial frequency was varied by a combination of viewing distance and software. The solid curves show the predictions of the IRC model (JS, = 0.54; AK = 0.67). Again the fits are

reasonably good (a little better for JS than AK) and the parameters are similar to those for the fits to the Robson and Graham data.

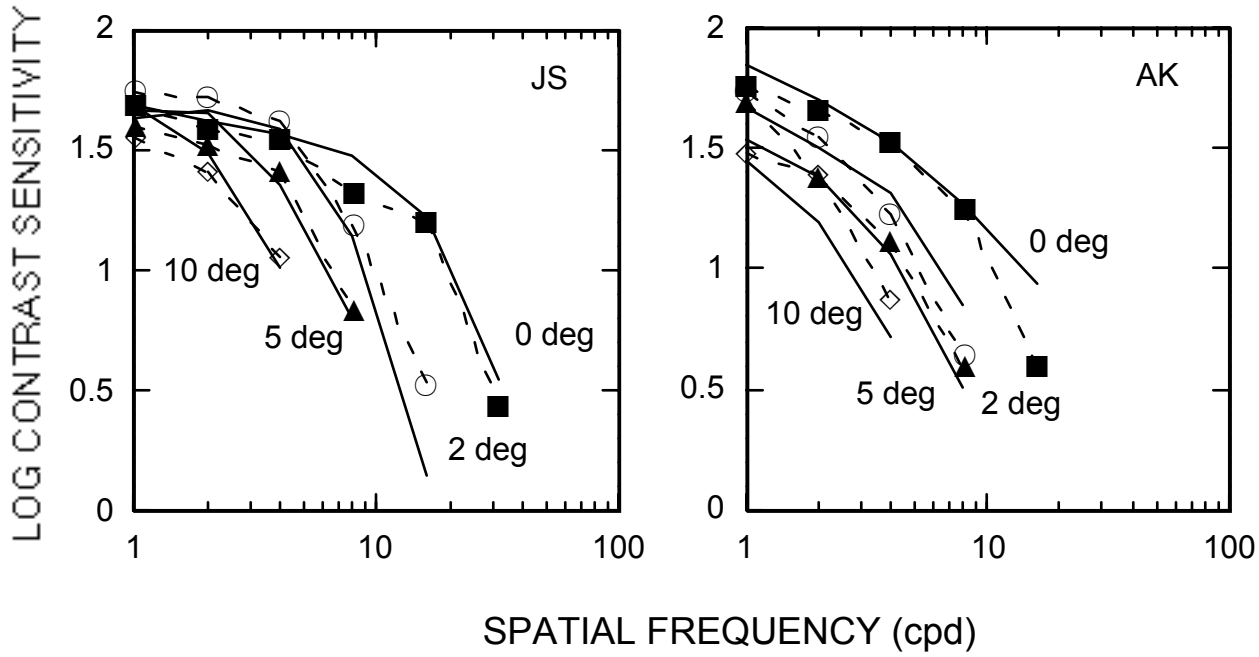

Figure 4. Contrast sensitivity for Gaussian-dampened sinewave grating targets as a function of spatial frequency and retinal eccentricity (data from Arnow and Geisler[2]). The targets were presented for 200 ms. The solid curves are the predictions of the IRC model.

Figure 5 shows the predictions of the IRC model for foveal contrast sensitivity, assuming circular scotomas with sharp boundaries. The predictions are for Gaussian-dampened sinewave gratings with a standard deviation of 1°. (Note that these targets are of fixed retinal size, not a fixed number of cycles.) The gratings were assumed to be centered on the fovea. The scotomas were assumed to vary in diameter from 0° to 10°, and to be located either in the fovea, at 2° eccentricity, or at 5° eccentricity. The model predicts that even relatively small scotomas will have a measurable effect on contrast sensitivity at all spatial frequencies (albeit a greater effect at high spatial frequencies). Also, not surprisingly, the model predicts the greatest effect for foveal scotomas,

3.2 Predictions for an "airplane" target

The predictions of the IRC model were also compared with contrast sensitivity measurements taken for a complex "airplane" target, with and without artificial circular scotomas with sharp boundaries. The target consisted of a scanned, side-view photograph of an F15C fighter jet, embedded in a gray background. The aspect ratio of the target was approximately 3.6. The background luminance and the mean luminance of the airplane were kept equal and constant at 130 cd/m^2. The contrast of the airplane target was controlled by manipulating the color look-up table. The area of the airplane target was varied over two orders of magnitude; i.e., the aspect ratio was fixed and the long axis of the airplane varied from 0.5° to 6° in visual angle. Target duration was 200 ms. Contrast thresholds for detecting the target were measured in a 2AFC task, using the same subjects and psychophysical procedures described earlier in connection with Figure 4.

The squares in Figure 6 show contrast sensitivity as a function of target size in the no-scotoma condition, for the two subjects. The circles and triangles show the measured contrast sensitivities for scotomas of 1° and 2° diameter, respectively. The solid, small-dashed, and large-dashed curves show the predictions of the IRC model for the three scotoma conditions, using the same parameters estimated from the measurements

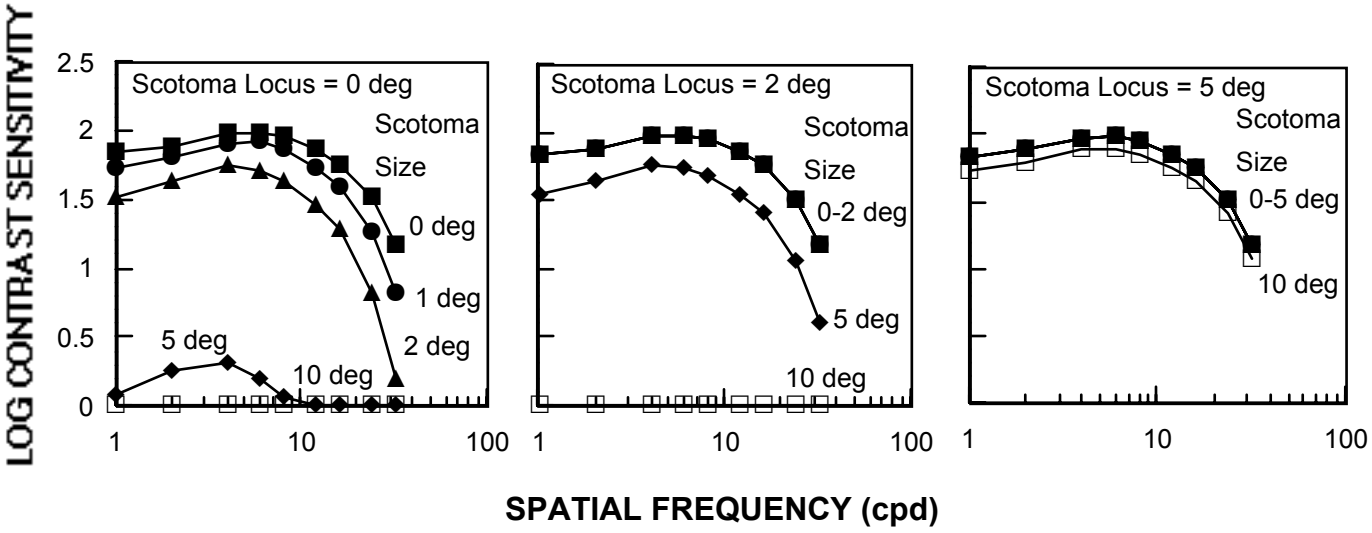

Figure 5. Predicted foveal contrast sensitivity for Gaussian-dampened sinewave grating targets which have an envelope standard deviation of 1°, as a function of spatial frequency, scotoma diameter, and scotoma eccentricity. The parameters were the same as those in the fit to the data of subject JS (see Figure 4).

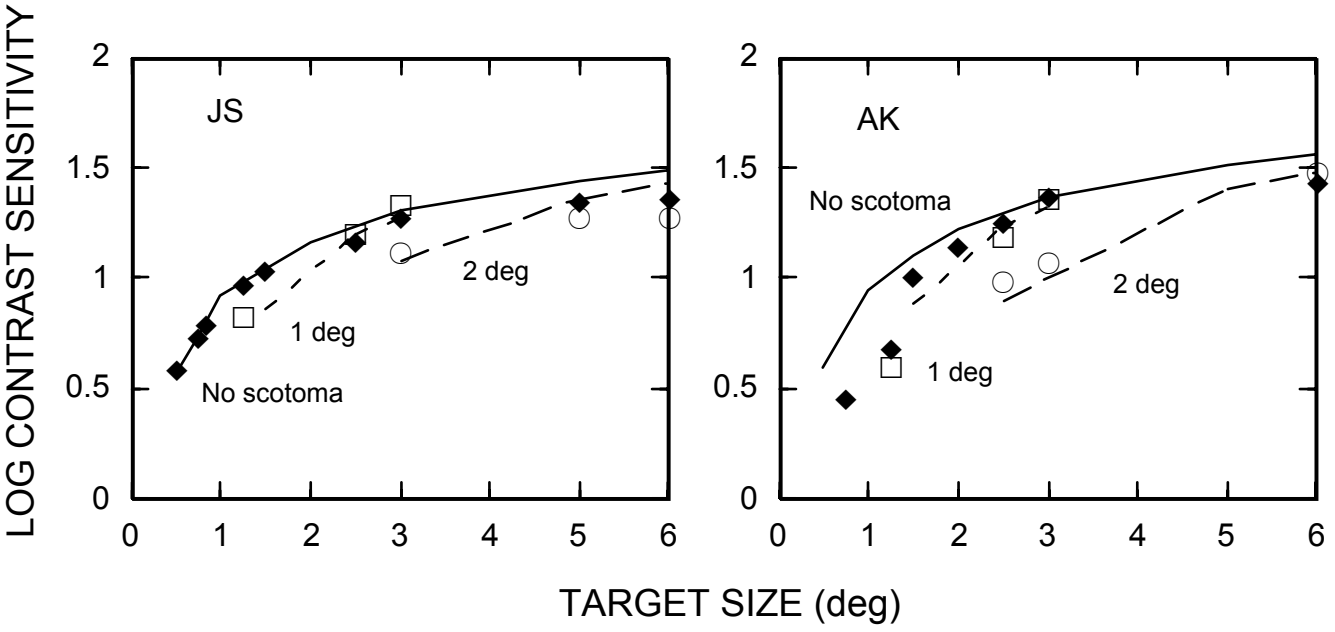

Figure 6. Contrast sensitivity for an airplane target as a function of target size, for three artificial scotoma conditions: no scotoma, a 1° central scotoma, a 2° central scotoma. The curves are the predictions of the IRC model, for the same parameters as Figure 4.

in Figure 4. The predicted curves for subject AK are untranslated, but those for subject JS have been translated downward by 0.25 log units for the purpose of comparing shapes. As can be seen, the model predicts the effects of target size and scotoma size relatively well. Specifically, it predicts the increase in

sensitivity with target size and predicts that there should be little effect of the scotoma until the target size is near or below the size of the scotoma (see the square at 1.5° and the open circle at 3°). We have no good explanation for why there is a small mismatch in the predicted absolute sensitivity for subject JS, but not for subject AK.

4.0 CONCLUSIONS

We have shown that a straight-forward model, based directly upon anatomical and physiological properties of the primate retina and primary visual cortex, does a reasonable job of predicting detection thresholds for sinewave grating patterns, as function of spatial frequency, size and retinal eccentricity. The model also did a reasonable job of predicting detection thresholds for a complex target as a function of target size and scotoma size. These encouraging results suggest that the IRC model (or a slightly modified version) may make accurate predictions of detection performance for a wide range of stimulus patterns. Further tests should not be difficult since the model has been implemented so that predictions can be generated for arbitrary patterns.

The current model was only designed to make predictions for detection of static patterns in uniform backgrounds. Current efforts are directed at expanding the model to include more properties of primary visual cortex. Inclusion of these properties will be necessary if the model is to make accurate predictions of pattern detection in cluttered backgrounds.

5.0 REFERENCES

[1] Robson, J. G., & Graham, N. (1981). Probability summation and regional variation in contrast sensitivity across the visual field. *Vision Research*, 21, 409-418.

[2] Arnow, T. L., & Geisler, W. S. (1995). Cycle summation in single and compound grating patterns. In *Association for Research in Vision and Opthalmology*, Fort Lauderdale.

[3] Charman, W. N. (1995). Optics of the eye. In M. Bass (Ed.), *Handbook of Optics* New York: McGraw-Hill.

[4] Geisler, W. S., & Banks, M. S. (1995). Visual Performance. In M. Bass (Ed.), *Handbook of Optics* New York: McGraw-Hill

[5] Campbell, F. W. & Gubish, R.W. (1966) Optical quality of the human eye. *Journal of Physiology*, 186, 558-578.

[6] Geisler, W. S., & Davila, K. D. (1985). Ideal discriminators in spatial vision: two-point stimuli. *Journal of the Optical Society of America A*, *2*, 1483-1497.

[7] Curcio, C. A., & Allen, K. A. (1990). Topography of ganglion cells in the human retina. *Journal of Comparative Neurology*, 300, 5-25.

[8] Merigan, W. H., & Maunsell, J. H. R. (1993). How Parallel are the primate visual pathways? *Annual Review of Neuroscience*, 16, 369-402.

[9] Derrington, A. M., & Lennie, P. (1984). Spatial and temporal contrast sensitivities of neurones in lateral geniculate nucleus of macaque. *Journal of Physiology*, 357, 219-240.

[10] Kaplan, E., & Shapley, R. (1986). The primate retina contains two types of ganglion cells, with high and low contrast sensitivity. *Proceedings of the National Academy of Sciences, USA*, 83, 125-143.

[11] Croner, L. J. & Kaplan, E. (1995). Receptive fields of P and M ganglion cells across the primate retina. *Vision Research*, 35 (1), 7-24.

[12] Wässle, H., Grünert, U., Röhrenbeck, J., & Boycott, B. B. (1990). Retinal ganglion cell density and cortical magnification factor in the primate. *Vision Research*, 30(11), 1897-1911.

[13] Watanabe, M. & Rodieck, R.W. (1989). Parasol and midget ganglion cells of the primate retina. *Journal of Comparative Neurology*, 289, 434-454.

[14] Albrecht, D. G., & Hamilton, D. H. (1982). Striate cortex of monkey and cat: contrast response function. *Journal of Neurophysiology*, 48(1), 217-237.

[15] Sclar, G., Maunsell, J. H. R., & Lennie, P. (1990). Coding of image contrast in central visual pathways of macaque monkey. *Vision Research*, 30, 1-10.

[16] Albrecht, D. G., & Geisler, W. S. (1991). Motion selectivity and the contrast-response function of simple cells in the visual cortex. *Visual Neuroscience*, 7, 531-546.

[17] Heeger, D. J. (1991). Computational model of cat striate physiology. In M. S. Landy & A. Movshon (Eds.), *Computational Model of Visual Perception* (pp. 119-133). Cambridge: The MIT press.

[18] DeValois, R. L., Albrecht, D. G., & Thorell, L. G. (1982). Spatial frequency selectivity of cells in macaque visual cortex. *Vision Research*, 22, 545-559.

[19] Tolhurst, D. J., Movshon, J. A., & Dean, A. F. (1983). The statistical reliability of signals in single neurons in the cat and monkey visual cortex. *Vision Research*, 23, 775-785.

[20] Geisler, W. S. & Albrecht, D. G. (1995) Bayesian Analysis of Identification Performance in Monkey Visual Cortex: Nonlinear Mechanisms and Stimulus Certainty. *Vision Research*, 35, 2723-2730.

[21] Green, D. M., & Swets, J. A. (1974). *Signal Detection Theory and Psychophysics.* New York: Krieger.

Notes and Acknowledgments

The experiments were conducted by TLA at Conceptual Mindworks Inc. The IRC model was developed by WSG at UT Austin. This work was supported by Armstrong Lab, Brooks AFB F41624-93-C-9015, AFOSR grant F49620-93-1-0307 (WSG), and NIH grant EY02688 (WSG).